*International Journal of Multidisciplinary and Current Research* ISSN: 2321-3124
Research Article Available at: http://ijmcr.com

# New Trend for Studying and Assessment of the Environmental and Health Risk using Real Time Gaussian Plume Model

**O.S. Ahmed*[1] and Khaled A. Salman[2]**

[1]Siting and Environmental Department, Radiological Control Division, Nuclear and Radiological Safety Research Center, Egyptian Atomic Energy Authority.
[2]Nuclear Research Center, Egyptian Atomic Energy Authority, Cairo, Egypt.

Received 01 Dec 2025, Accepted 12 Dec 2025, Available online 15 Dec 2025, **Vol.13 (Nov/Dec 2025 issue)**

***Abstract***

*Nuclear power plants can release radionuclides to the atmosphere under normal operating conditions or during abnormal events. As a consequence, atmospheric dispersion and concentration calculations for routine and accidental releases of radioactive materials are required to assess the dispersion of radioactive materials, this concentration calculations are affected by several parameter. This paper focus on study the effect of receptor height, wind direction and atmospheric stability upon the concentration for radionuclides released from NPP site using real-time Gaussian plume model ( free license), which this parameters are important to assess the dispersion of radioactive materials, where important for licensing requirements for any nuclear facility , Designing monitoring, surveillance systems and developing atmospheric dispersion models, which used for estimating radiological evaluation and finally for Setting emergency plane in case accident. The results indicated the feasibility of applying the code for developing training programs for students, and consequently efficient use of the limited resources to achieve innovative teaching method for air dispersion programs, our results for this study are shown with application.*

***Keywords:*** *Atmospheric Dispersion, Wind Direction, Stability Class, Receptor Height, Emergency Plane, The Gaussian Plume Model*

## Introduction

Air quality and possible health and environmental effects are determined by the dispersion of pollutants. Environmental and health risk assessment is a crucial element in the planning and execution phases of any chemical, nuclear, or industrial project. Its objectives include lowering the probability of environmental mishaps or disasters and identifying possible effects on people and the environment. This assessment also helps to create scientific standards for choosing the best project locations, guaranteeing a balance between public health, environmental preservation, and economic development. Finding the sources of hazards, such as gaseous emissions, radioactive materials, chemical pollutants, or industrial waste, is one of the assessment steps, investigating the methods by which contaminants enter the atmosphere, water, or soil and make their way to people or other living things, Risk characterization involves figuring out the pollution levels and exposure times.

Selecting the right location requires a thorough examination of environmental, geographical, and social factors, the most crucial of which are wind directions and atmospheric stability, which limit the spread of pollutants to residential areas; distance from water sources and residential and agricultural areas; and terrain features, such as mountains and valleys, which have an impact on air movement and the spread of pollutants. Estimating the movement and dispersion of pollutants in the atmosphere is done using atmospheric dispersion models, which are an essential tool for assessing pollutant concentrations in various locations and assisting decision-makers. [1-5]

## Theoretical Background

For dispersion calculations needed study effect some parameters such as wind direction, atmospheric stability and receptor height , where this parameters plays significant roles in determining the concentration of pollutants at various locations in the atmosphere, where Atmospheric stability is considered one of the most important factors affecting the spread and dissipation of air pollutants, as it increases the concentrations of pollutants in a certain layer, prevents their dispersion, and at other times works to spread them and reduce their

*Correspondant Author's ORCID ID: 0009-0000-0000-0000
DOI: https://doi.org/10.14741/ijmcr/v.13.6.4

concentration, Since stability and its varieties depend primarily on weather factors, which differ according to the season of the year , To classify atmospheric stability to six classes designated A (extremely unstable) to F (moderately stable), the most widely used scheme is originated by Pasquill as shown in table(1),where stability conditions are divided [6-13], the second parameter is wind direction ,which determines how pollutants move horizontally in the atmosphere, and it can significantly impact where pollutants accumulate and how concentrated they are at any given location, the radioactive materials moved corresponding to the prevailing wind and the final parameter is the height of the receptor (the location where the pollutant concentration is being measured) is an important factor because the concentration of pollutants typically varies with height above the ground. The effect of receptor height is influenced by both stability and wind direction. most estimates for concentration are based on the Gaussian plum e diffusion model, The Gaussian plume model approach as fig (1) is the most widely used method of estimating downwind concentrations of airborne material released to the atmosphere. In the application of this model, which has been verified under widely different meteorological conditions, the plume spread has a Gaussian distribution in both the horizontal and vertical and, therefore, utilizes the standard deviations of plume concentration distribution in the horizontal$\sigma_y$ and vertical $\sigma_z$ [9] for estimating concentrations for release periods of nominally one hour in accordance with a Gaussian distribution as equation (1) [14-23]

$$\mathbf{X(x,y,z)} = \frac{\mathbf{Q}}{\mathbf{2\Pi\ \sigma_y\ \sigma_z\ U}}\ \mathbf{exp}\left[-\left(\frac{\mathbf{Y^2}}{\mathbf{2\sigma_{\bar{y}}^2}}\right)\right]\ \left(\mathbf{exp}\left[-\left(\frac{\mathbf{-(z-h)^2}}{\mathbf{2\sigma_{\bar{z}}^2}}\right)\right] + \mathbf{exp}\left[-\left(\frac{\mathbf{-(z+h)^2}}{\mathbf{2\sigma_{\bar{z}}^2}}\right)\right]\right)$$

Where,

X(x,y,z): air concentration (Bq.m-3) at a point with coordinates x,y,z,
x: downwind distance(m),
y: crosswind distance (m),
z: height above the ground (m),
Q: release rate ((Bq.s-1)
U: mean wind speed ((m.s-1)
h: effective release height (m)
$\sigma_y$ $\sigma_z$ : Diffusion parameters (m), which are a function of downwind distance, x, and atmospheric stability.

**Table 1** Key to stability categories

| Wind speed U (m.s-1) at 10 m | Stability class, day, with solar radiation $R_D$ (langleys.h$^{-1}$) | | | | | Stability class, night, with net radiation $R_N$ (langleys.h$^{-1}$) | |
|---|---|---|---|---|---|---|---|
| **Wind speed U (m·s$^{-1}$)** | **$R^D \geq 50$** | **$50 > R^D \geq 25$** | **$25 > R^D \geq 12.5$** | **$12.5 > R^D$** | **$R^N > -1.8$** | **$-1.8 \geq R^N > -3.6$** | **$-3.6 \geq R^N$** |
| U < 2 | A | A–B | B | D | D | E | F |
| 2 ≤ U < 3 | A–B | B | C | D | D | E | F |
| 3 ≤ U < 4 | B | B–C | C | D | D | D | E |
| 4 ≤ U < 6 | C | C–D | D | D | D | D | D |
| U ≥ 6 | C | D | D | D | D | D | D |

Where

A – Extremely unstable, B – Moderately unstable, C – Slightly unstable, D – Neutral, E – Slightly stable, F – Moderately stable

**Case Study**

Let us consider hypothetical data for a facility with the release rate as shown in Table 2.

**Table 2** Parameter values for study case used in Real –time Gaussian Dispersion

| | |
|---|---|
| **Downwind distance to calculate (1–50 km)** | 5 |
| **Source latitude** | 30.13 |
| **Source longitude** | 31.40 |
| **Source height (0–100 meters AGL)** | 50 |
| **Release rate (units/second)** | 100 |
| **Receptor height (meters AGL)** | 60 |
| **Start of release (UTC/GMT time)** | Hour: **12** Day: **15** Month: **6** Year: **2020** |
| **Cloud cover (% covered)** | 50 |
| **Wind direction (deg)** | 0 |
| **Wind speed** | 5.0 |
| **Wind speed units** | ◉ m/s ○ knots ○ mph |
| **Cloud ceiling (feet, use 20000 if not known)** | 20000 |
| **Mixing depth (meters AGL, default [0] will compute it)** | 0 |
| **Maximum nighttime mixing depth (meters AGL)** | 400 |
| **Maximum daytime mixing depth (meters AGL)** | 5000 |
| **Graphic size (dpi)** | ◉ 72 ○ 96 ○ 120 |
| **Create Postscript file?** | ○ Yes ◉ No |
| **Create GIS output of contours?** | ○ None ◉ GIS Shapefiles ○ Google Earth (kmz) |

Gaussian Dispersion with User Data
Source Location: Cairo, Latitude: 30.13, Longitude: 31.40

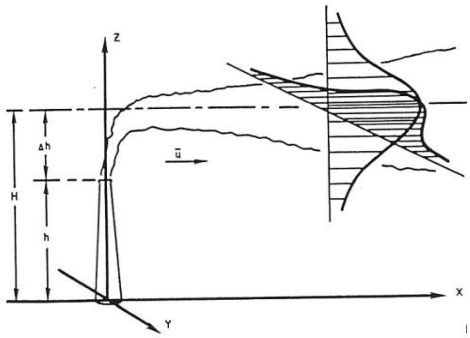


**Figure 1** Gaussian Dispersion Model

## Results and Discussion

### Study Effect of receptor height on dispersion of radionuclides

Figures 2–8 present the results of the centerline peak concentration (s/m³) of released radionuclides for the study region located at 30.13°N, 31.40°E, under identical meteorological conditions. The analysis considers different receptor heights: ground level (no building), half the source height, equal to the source height, one and a half times the source height, and twice the source height.

Figure 2 illustrates the dispersion pattern of airborne radionuclides generated using the Gaussian Plume Model. The release occurred on 15 June 2020 at 12:00 UTC from the specified coordinates and continued for six hours. The colored contours represent concentration levels (s/m³), with the highest concentrations shown in red near the source. As the plume moves downwind, concentrations progressively decrease through orange, yellow, green, blue, and violet regions, indicating plume dilution. The centerline peak concentration is approximately $1.2 \times 10^{-3}$ s/m³ at 0.5 km after about 2 minutes, decreasing to $7.6 \times 10^{-5}$ s/m³ at 2 km after 9 minutes, and further reducing to $1.6 \times 10^{-5}$ s/m³ beyond 5 km after 23 minutes. These results demonstrate that the highest risk zone lies close to the release point, with concentrations decreasing rapidly due to atmospheric mixing.

Figure 3 shows pollutant concentration contours expressed in s/m³. The maximum concentration (≈ $1.0 \times 10^{-3}$ s/m³) appears in the red zone within approximately 0.5 km downwind of the source. Moderate concentrations extending up to 2–3 km are represented by yellow and green regions, while the blue zone indicates low concentrations beyond 4 km. The centerline peak values further confirm the rapid decay of concentration with distance, emphasizing the roles of atmospheric turbulence, diffusion, and advection in plume dilution.

Figure 4 represents dispersion under unstable atmospheric conditions (Class B). The plume spreads rapidly in both vertical and horizontal directions, resulting in reduced concentrations farther downwind. The highest concentrations are confined to the first kilometer, indicating that areas closest to the source experience the greatest exposure risk.

Figure 5 illustrates the dispersion pattern when the receptor height is 1.5 times the source height (receptor = 75 m, source = 50 m). The plume contours show decreasing concentrations outward from the source, with the highest values (≈ $10^{-3}$ s/m³) occurring within 0.5 km. Because the receptor is elevated above the stack height, it intersects the plume closer to its centerline, where concentrations are higher. Consequently, the observed concentration at the receptor increases before vertical diffusion reduces plume intensity.

Figure 6 depicts the case where the receptor height is twice the source height (receptor = 100 m, source = 50 m). Compared to Figure 5, the plume exhibits wider vertical dispersion as it travels downwind. Although the receptor height is increased, the centerline concentration decreases because the receptor begins to move above the plume core. Enhanced vertical mixing dominates, resulting in weaker concentration gradients near the source.

Figure 7 demonstrates that the observed centerline concentration decreases as receptor height increases. Maximum concentrations occur very close to the source and at lower receptor elevations. Overall, this figure confirms that pollutant concentration is inversely related to both receptor height and distance, with maximum exposure occurring near the emission point and close to ground level.

Figure 8 examines the variation of centerline concentration with receptor height while maintaining a constant source height (50 m) and downwind distance (0.5 km). At low receptor heights, concentrations remain high and nearly constant (≈ $1.2 \times 10^{-3}$ s/m³). As the receptor height increases above the stack height, concentrations gradually decrease, reaching approximately $6.2 \times 10^{-5}$ s/m³ at twice the stack height. This behavior occurs because the plume center—where concentration is highest-is typically located near or slightly above the stack height. Elevating the receptor beyond this level moves it away from the plume core, resulting in increased dilution and reduced concentration.

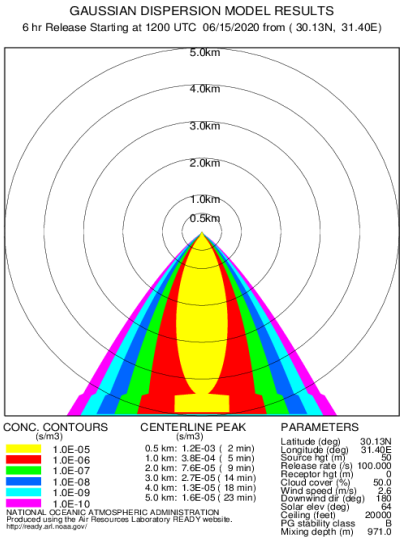


**Figure 2** Centerline peak of concentration (s/m3) at receptor height is zero

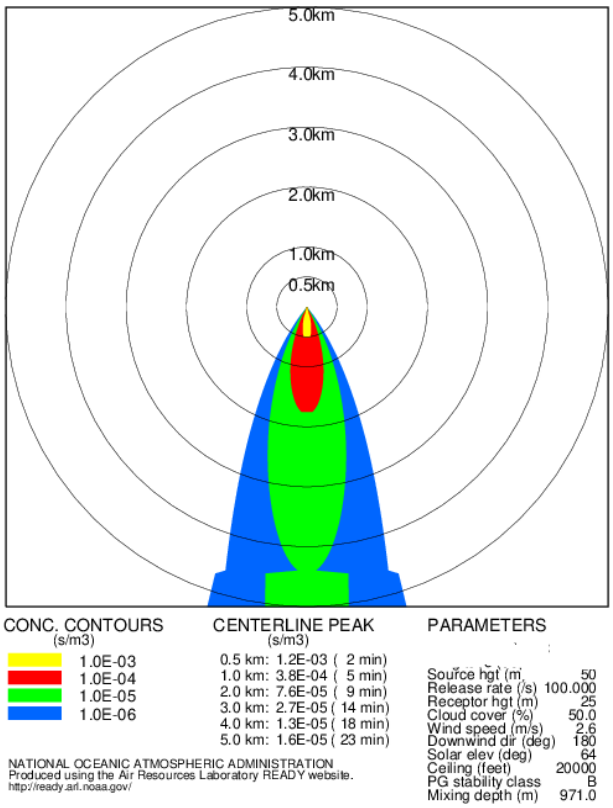


**Figure 3** Centerline peak of concentration (s/m3) at receptor height is half

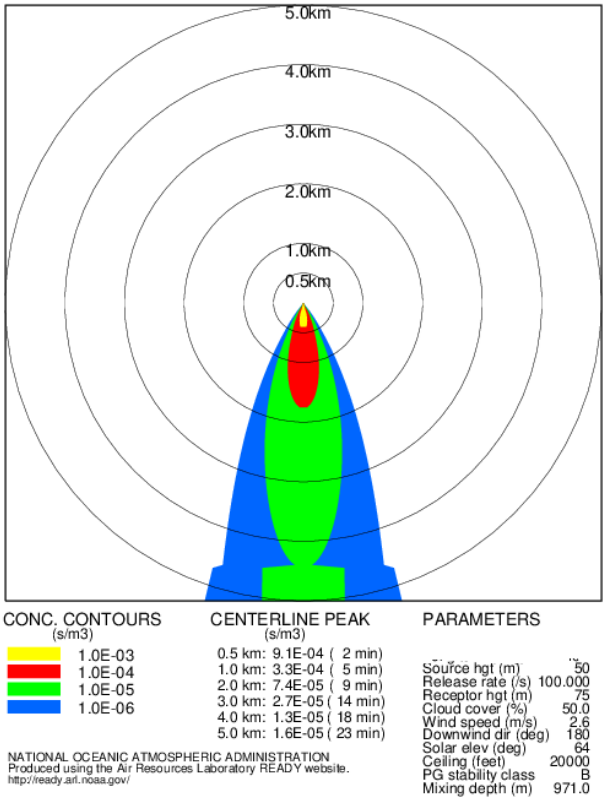


**Figure 5:** Centerline peak of concentration (s/m3) at receptor height is *one and a half times larger* the source height

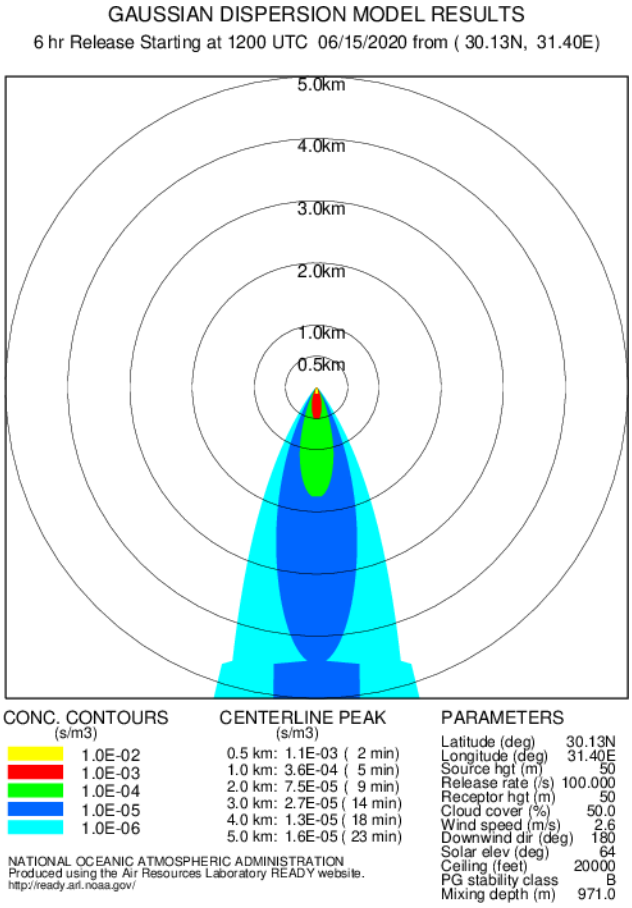


**Figure 4** Centerline peak of concentration (s/m3) at receptor height is equal source height

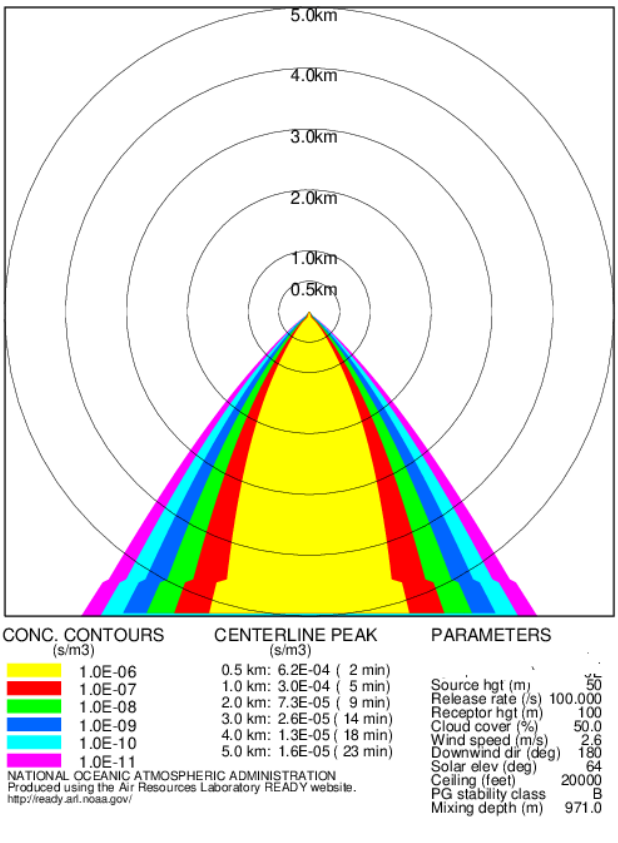


**Figure 6** Centerline peak of concentration (s/m3) at receptor height is twice *bigger* of source height

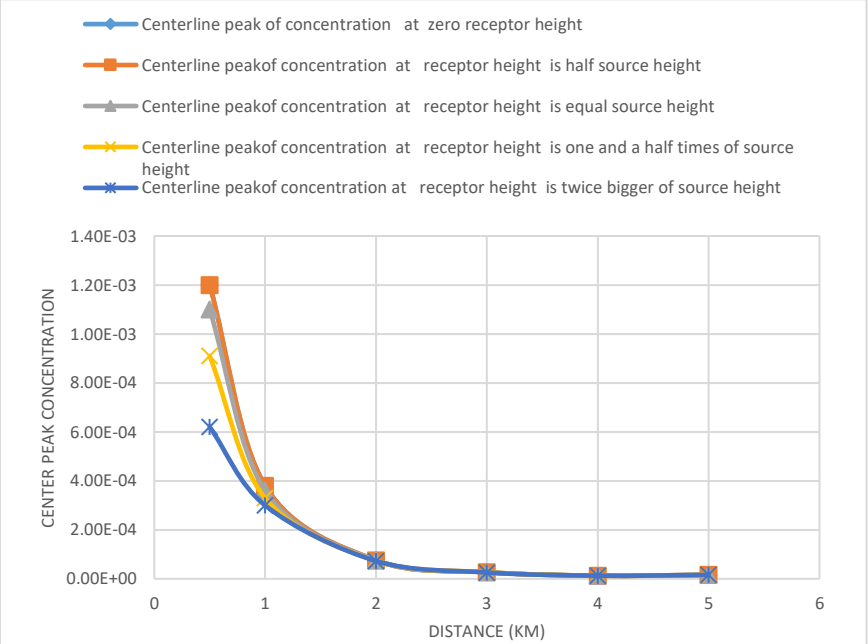


**Figure 7** Centerline peak of concentration (s/m3) at different value of receptor height

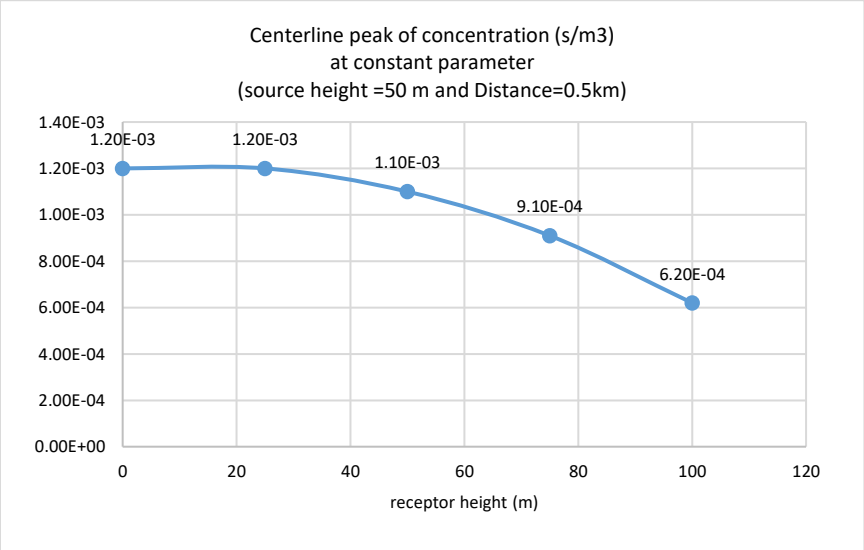


**Figure 8** Centerline peak of concentration (s/m3) at different value for receptor height at constant value of source height and Distance from release point

**Table 3** The result of Centerline peak of concentration at different value for receptor height and distances from release point

| D (km) | Centerline peak of concentration at zero receptor height | Centerline peak of concentration at receptor height is half source height | Centerline peak of concentration at receptor height is equal source height | Centerline peak of concentration at receptor height is one and a half times of source height | Centerline peak of concentration at receptor height is twice bigger of source height |
|---|---|---|---|---|---|
| 0.5 | 1.20E-03 | 1.20E-03 | 1.10E-03 | 9.10E-04 | 6.20E-04 |
| 1 | 3.80E-04 | 3.80E-04 | 3.60E-04 | 3.30E-04 | 3.00E-04 |
| 2 | 7.60E-05 | 7.60E-05 | 7.50E-05 | 7.40E-05 | 7.30E-05 |
| 3 | 2.70E-05 | 2.70E-05 | 2.70E-05 | 2.70E-05 | 2.60E-05 |
| 4 | 1.30E-05 | 1.30E-05 | 1.30E-05 | 1.30E-05 | 1.30E-05 |
| 5 | 1.60E-05 | 1.60E-05 | 1.60E-05 | 1.60E-05 | 1.60E-05 |

Table (3) explains how, under neutral stability (class D), the centerline peak concentration (s/m³) varies with both receptor height and distance from the release point. The concentration is maximum (around $1.2\times10^{-3}$ s/m³) for low receptor heights at short distances (0.5 km), indicating considerable exposure close to the ground. The concentration gradually drops as the distance increases because of the plume's dispersion and dilution. Similarly, as the final column illustrates, increasing receptor height (up to twice the source height) results in a decrease in concentration. These findings verify that the largest exposure happens near the source and close to the ground, and that it decreases with distance both vertically and horizontally. Table (4) demonstrates how changing the receptor height affects the centerline peak concentration while maintaining the same source height (50 m) and distance (0.5 km). According to the data, the concentration stays nearly constant (≈$1.2\times10^{-3}$ s/m³) until the receptor height equals the source height, after which it steadily decreases as the receptor height rises. The concentration falls to $6.2\times10^{-2}$ s/m³ at twice the source height (100 m), which is nearly half the value close to the ground. This pattern suggests that more dilution and plume rise result in lower concentrations for higher receptors. As a result, receptors at ground level are more at danger of exposure, whilst those at higher elevations are less contaminated.

**Table 4** The result of Centerline peak of concentration at different value for receptor height at constant value of source height (50 m) and distances from release point (0.5 km)

| receptor height (m) | Centerline peak of concentration (s/m3) |
|---|---|
| 0 | 1.20E-03 |
| 25 | 1.20E-03 |
| 50 | 1.10E-03 |
| 75 | 9.10E-04 |
| 100 | 6.20E-04 |

**Study Effect of atmospheric stability on dispersion of radionuclides for region (30 13 N, 3140E)**

Figure 9*:* shows the plume's dispersion when the atmosphere is categorized as stability class C, which indicate somewhat unstable daytime conditions. The broader green and blue contours indicate that the plume expands moderately in both vertical and horizontal directions. Pollutants can rise and disperse rapidly due to the enhancement of mixing caused by thermal turbulence from solar heating. As a result, compared to more stable conditions, the plume extends farther downwind and the maximum concentration near the source is mild. When convective mixing is active but not severe, these conditions typically arise in the middle of the morning or late afternoon. Figure 10: shows plume dispersion under stability class D, which corresponds to neutral air conditions and is usually present on cloudy or windy days. Because there is less convective activity than in class C, the plume in this instance is narrower and more vertically restricted. Limited vertical diffusion is shown by the concentration contours, which display a longer but thinner plume. This stability class results in intermediate dispersion, where contaminants travel farther and stay in the air longer before becoming significantly diluted.

These neutral conditions, which provide a continuous but less turbulent dispersion, frequently occur in the evening or during bad weather.

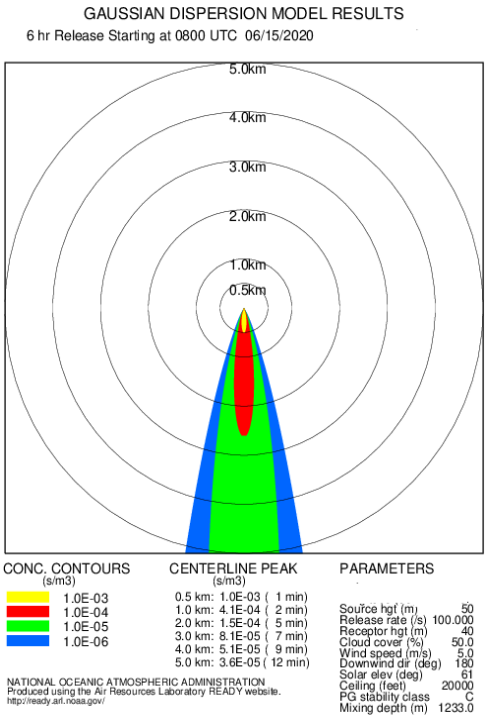


**Figure 9** Spread of plume in the stability class C condition

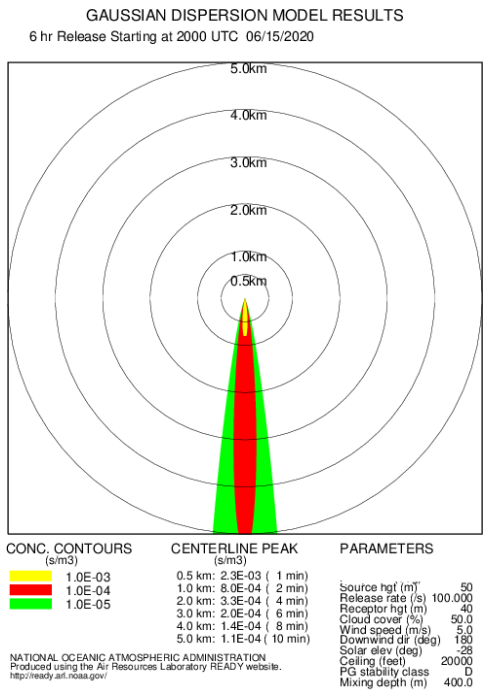


**Figure 10** Spread of plume in the stability class D condition

**3-Study Effect of wind direction for region (30 13 N, 3140E) on dispersion of radionuclides**

Figure 11 shows how the plume behaves under neutral stability (class D) when the wind blows straight north (0°). The plume exhibits a symmetrical, restricted distribution with little lateral spread while staying aligned along the wind axis. There is little crosswind diffusion due to the neutral atmosphere and constant wind direction, which results in a strong concentration gradient close to the plume centerline. As a result, the majority of the radioactive material stays concentrated over a narrow downwind path. This illustrates how contamination can be concentrated over a particular geographic region by a consistent wind direction, Figure 12: demonstrates the same wind direction (0°) in more erratic circumstances (class C). The plume is broader and more dispersed than in Figure 11, suggesting more intense vertical and horizontal turbulence. Green and blue zones quickly replace the red zone (high concentration) close to the source, indicating increased dilution as a result of instability.

The peak centerline concentration decreases as the plume disperses more widely in the crosswind direction. This demonstrates how unstable conditions encourage quicker diffusion of pollutants, reducing concentrations close to the source while impacting a wider area. *Figure 13:* In a neutral atmosphere (class D), this figure examines the plume as the wind direction changes to 90° (eastward). With a narrow vertical contour, the plume now stretches horizontally eastward. The symmetrical contours show that there is negligible crosswind deflection and the pollutant path closely follows the wind vector. The radionuclide cloud is concentrated along its main axis as a result of the neutral stability, which causes the plume to travel farther before dispersing considerably. This situation exemplifies a typical steady - state dispersion in which wind direction, not air turbulence, dominates the transport pathway.

Figure 14 displays the same 90° wind direction, but under **slightly unstable conditions (class C)**. In comparison to the neutral situation, the plume appears wider and more distributed in both vertical and horizontal directions (Figure 13). A fan-shaped plume that spans a greater region downstream is produced when stronger turbulence increases vertical lifting. The shorter length of the peak concentration zone (red region) indicates lower intensity and faster dilution close to the source. Overall, this figure shows that crosswind flow and unstable conditions encourage effective dispersion, decreasing localized exposure while enlarging the impacted area.

Figure 15 demonstrates how the plume expands under neutral atmospheric stability (class D) when the wind direction is 180° (southward). Because of neutral stability conditions, the plume appears thin, elongated, and symmetric, suggesting low vertical and lateral mixing. Diffusion is moderate and the majority of the radionuclide concentration stays oriented along the wind axis. The plume stays reasonably well-confined vertically, with greatest concentration close to the source and progressive diminution along the downwind direction, because stability class D is associated with cloudy or windy conditions. This illustrates how the plume trajectory is extremely reliant on wind direction under neutral stability, leading to directionally directed dispersion.

Figure 16 represents the same 180° (southward) wind flow but under slightly unstable atmospheric conditions (class C). Due to greater thermal turbulence, the plume is wider and more dispersed than in Figure (15), exhibiting notable vertical and horizontal dispersion. The red area close to the release point, which denotes a higher concentration, rapidly disappears into green and blue outlines, signifying a speedy dilution of contaminants. Buoyant updrafts improve mixing in unstable conditions, increasing the impacted region while lowering the maximum concentration close to the ground. As a result, radionuclide dispersion widens and becomes less concentrated under class C, indicating that instability encourages faster dilution and wider spread. Figure (17): In this figure, neutral atmospheric stability (class D) is maintained as the wind direction changes to 270° (westward).

The plume has a narrow, elongated shape with little lateral expansion as it stretches horizontally toward the west. The constant wind flow with minimal vertical turbulence is reflected in this shape, which enables the plume to travel great distances before noticeably dispersing. Consequently, the centerline concentration steadily decreases with distance and stays high close to the source. This example demonstrates that, under neutral conditions, the direction of the wind mostly determines the contamination path's orientation, with diffusion remaining comparatively sluggish.

Figure 18 The same westward (270°) wind direction is shown in this figure, although under somewhat erratic circumstances (class C). The plume is shorter and wider than in Figure (17), which indicates more intense turbulent mixing. Enhanced diffusion in both vertical and horizontal directions is indicated by the contour sections (red, green, and blue) spreading farther laterally. Radionuclide particles mix rapidly as a result of increased atmospheric instability, which lowers peak concentrations and speeds up plume dilution. By encouraging quick dilution, air instability can lessen radiation exposure intensity close to the source, as this figure highlights.

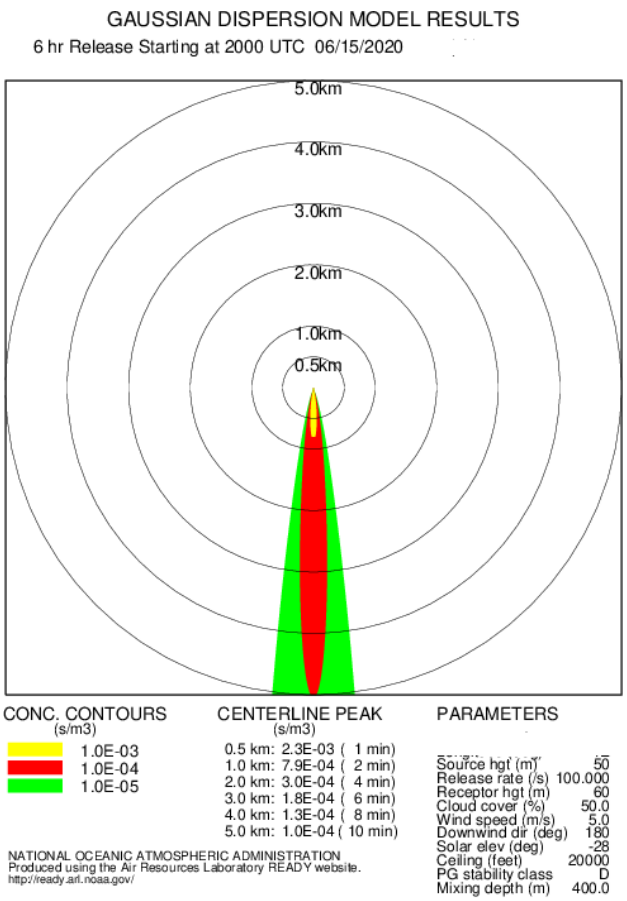


**Figure 11** Effect wind direction (0°) on dispersion of radionuclides at D stability class

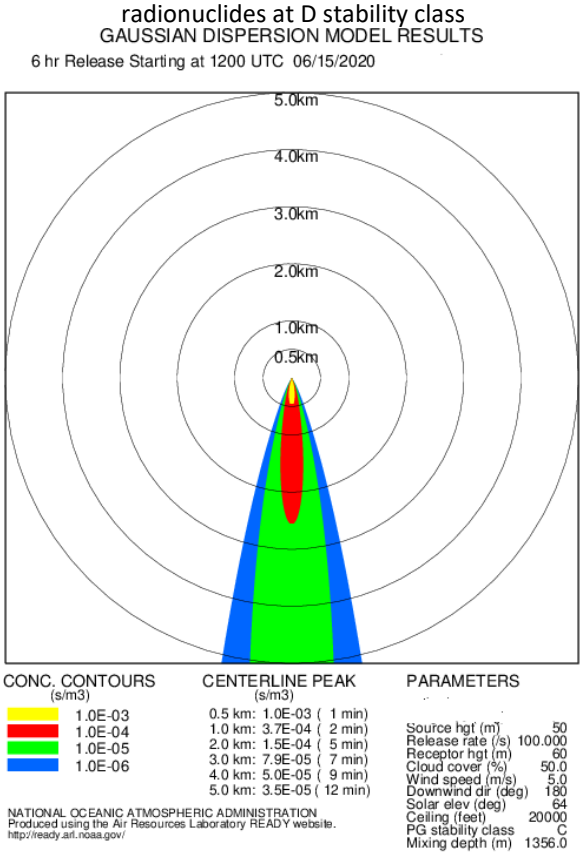


**Figure 12** Effect wind direction (0°) on dispersion of radionuclides at C stability class

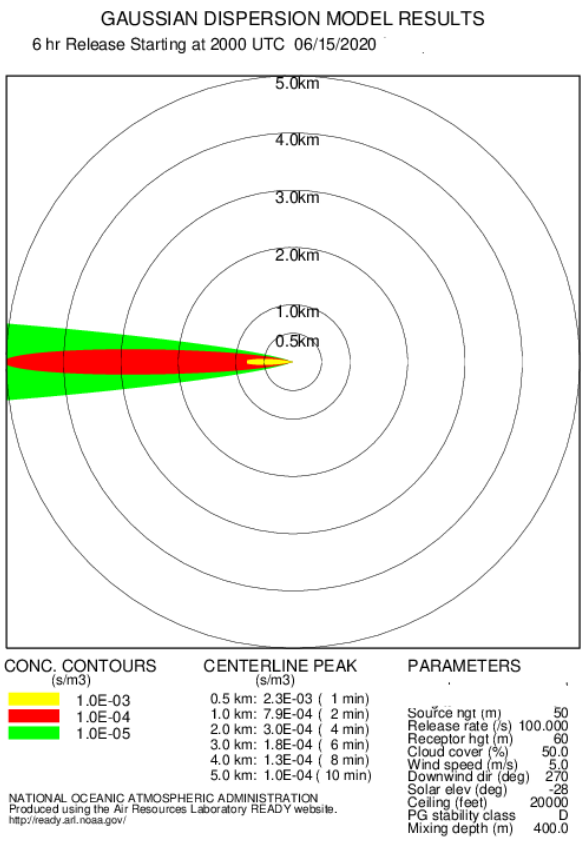


**Figure 13** Effect wind direction (90°) on dispersion of radionuclides at D stability class

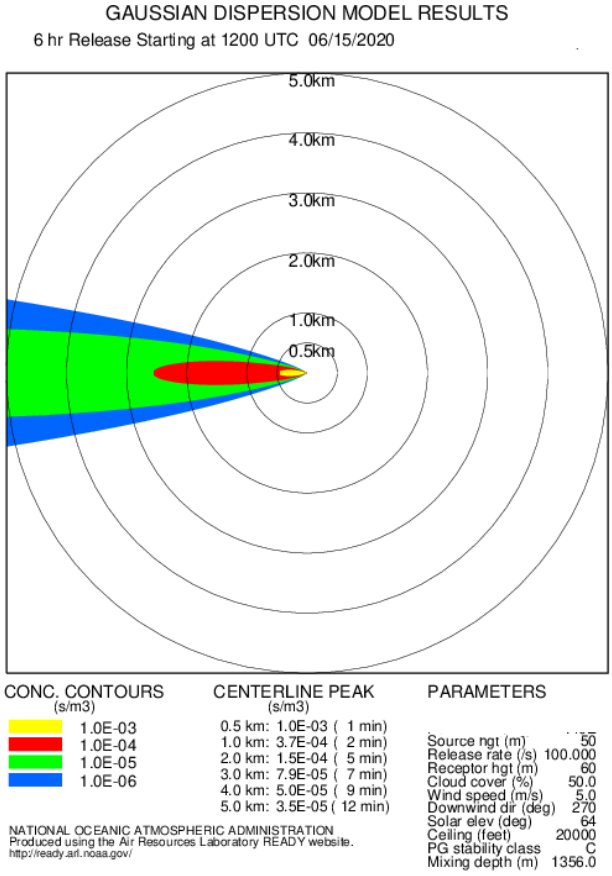


**Figure 14** Effect wind direction (90°) on dispersion of radionuclides at C stability class

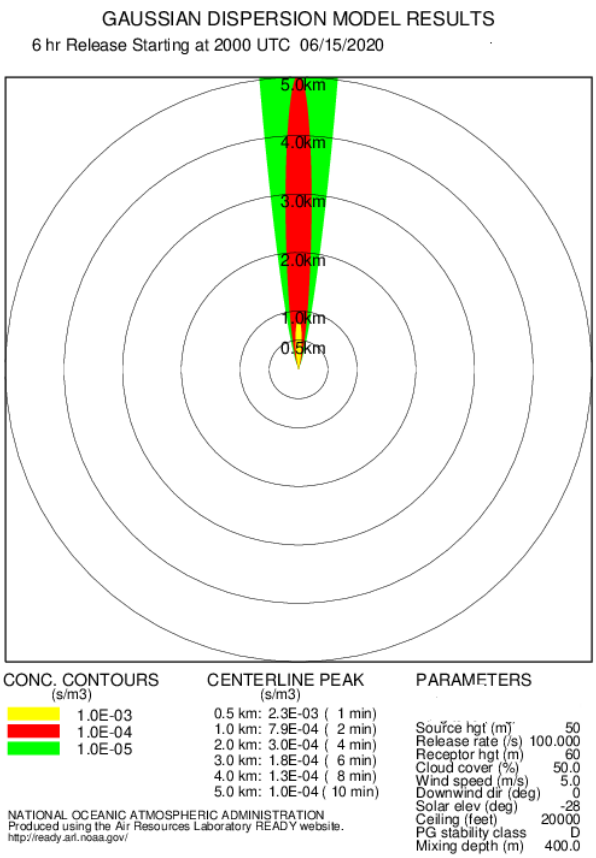


**Figure 15** Effect wind direction (180°) on dispersion of radionuclides at D stability class

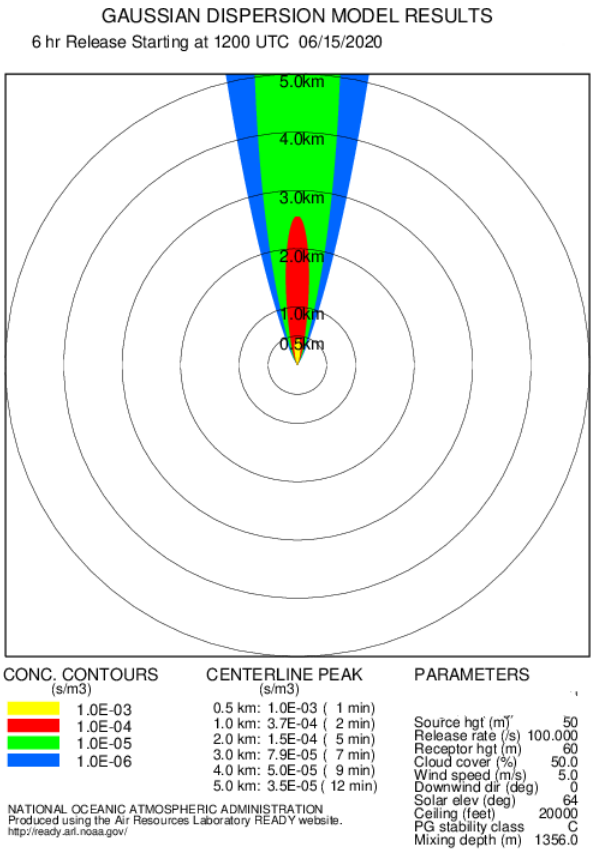


**Figure 16** Effect wind direction (180°) on dispersion of radionuclides at C stability class

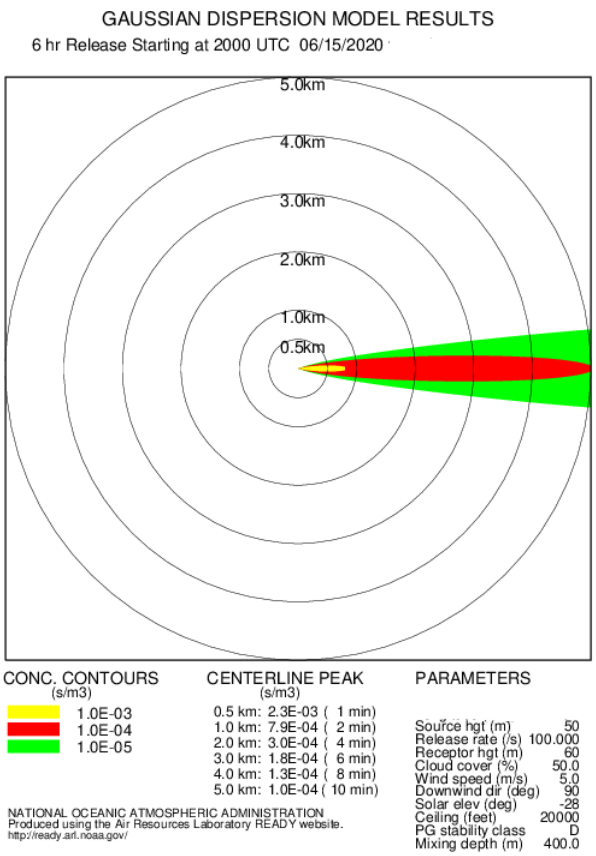


**Figure 17** Effect wind direction (270°) on dispersion of radionuclides at D stability class

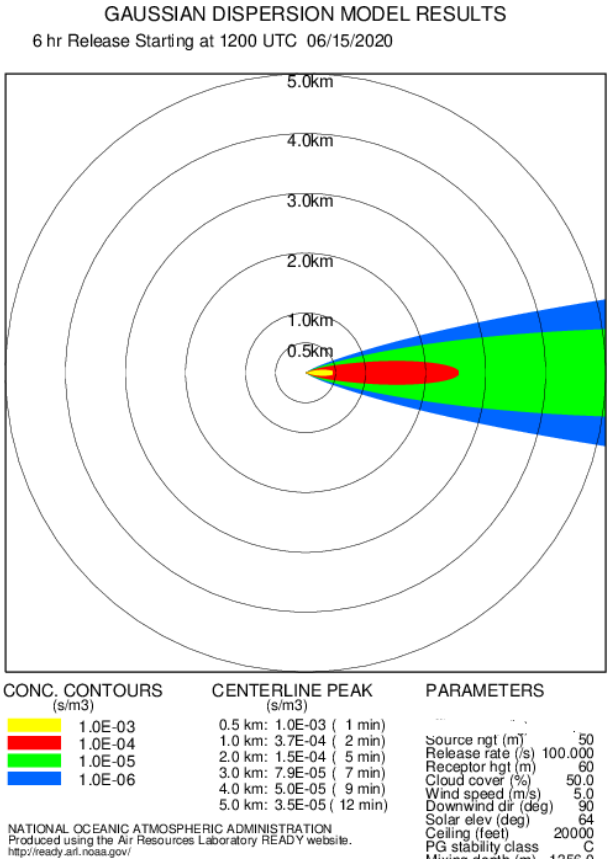


**Figure 18** Effect wind direction (270°) on dispersion of radionuclides at C stability class

## Conclusion

In this study, a real-time Gaussian plume model was used to investigate the influence of receptor height, wind direction, and atmospheric stability on the dispersion of radionuclides. These parameters are critical for several applications, including environmental and human health risk assessment, urban planning, optimal site selection for projects, development of monitoring and surveillance systems, pollutant dispersion modeling, and emergency response planning. The results indicate that receptor height, atmospheric stability, and wind direction significantly affect radionuclide diffusion and dispersion. Due to plume downwash, radionuclide concentration decreases as receptor height increases, reaching its maximum when the receptor is located near ground level. Stable atmospheric conditions (Class D) limit atmospheric mixing, resulting in higher concentrations near the emission source. In contrast, unstable atmospheric conditions (Class C) enhance turbulence, leading to greater plume dispersion and lower radionuclide concentrations. Furthermore, wind direction plays a crucial role in determining downwind spread and concentration levels. Under neutral atmospheric conditions, the plume is less dispersed compared to unstable conditions, which directly influences the spatial distribution of radionuclides. Overall, increasing receptor height is identified as an effective strategy for reducing pollution exposure at nuclear facilities.

## References

[1] J. E. Till and H. Grogan, Radiological Risk Assessment and Environmental Analysis. Oxford, U.K.: Oxford University Press, 2008.

[2] C. V. Srinivas, R. Venkatesan, R. Baskaran, V. Rajagopal, and B. Venkatraman, “Regional scale atmospheric dispersion simulation of accidental releases of radionuclides from Fukushima Dai-ichi reactor,” Atmospheric Environment, vol. 61, pp. 66–84, 2012.

[3] M. Hachem, N. Saleh, A. C. Paunescu, I. Momas, and L. Bensefa-Colas, “Exposure to traffic air pollutants in taxicabs and acute adverse respiratory effects: A systematic review,” Science of the Total Environment, vol. 693, Art. no. 133439, 2019.

[4] S. Zheng, J. Wang, C. Sun, X. Zhang, and M. E. Kahn, “Air pollution lowers Chinese urbanites’ expressed happiness on social media,” Nature Human Behaviour, vol. 3, pp. 237–243, 2019.

[5] D. Cui, X. Li, J. Liu, L. Yuan, C. M. Mak, Y. Fan, and L. Kwok, “Effects of building layouts and envelope features on wind flow and pollutant exposure in height-asymmetric street canyons,” Building and Environment, vol. 205, Art. no. 108177, 2021.

[6] Z. Shen, G. Cui, and Z. Zhang, “Turbulent dispersion of pollutants in urban-type canopies under stable stratification conditions,” Atmospheric Environment, vol. 156, pp. 1–14, 2017.

[7] D. Guo, F. Yang, X. Shi, Y. Li, and R. Yao, “Numerical simulation and wind tunnel experiments on the effect of a cubic building on the flow and pollutant diffusion under stable stratification,” Building and Environment, vol. 205, Art. no. 108222, 2021.

[8] C. Leroy, D. Maro, D. Hebert, et al., “A study of the atmospheric dispersion of a high release of krypton-85 above a complex coastal terrain: Comparison with Gaussian models (Briggs, Doury, ADMS4),” Journal of Environmental Radioactivity, vol. 101, pp. 937–944, 2010.

[9] Q. Zhang, R. Guo, C. Zhang, et al., “Radioactive airborne effluents and environmental impact assessment of the CAP1400 nuclear power plant under normal operation,” Nuclear Engineering and Design, vol. 280, pp. 579–585, 2014.

[10] A. F. Hassoon, S. K. Mohammed, and H. H. H. Al-Saleem, “Atmospheric stability and its effect on polluted concentration columns in northwest Baghdad city,” Iraqi Journal of Science, vol. 55, pp. 572–581, 2014.

[11] M. T. Kiefer et al., “Development of a wind and Pasquill stability class climate dataset for the North American Great Lakes region,” 2022.

[12] K. B. Schnelle and P. Dey, Atmospheric Dispersion Modeling Compliance Guide. New York, NY, USA: McGraw-Hill, 2000.

[13] International Atomic Energy Agency (IAEA), Environmental Consequences of the Chernobyl Accident and Their Remediation: Twenty Years of Experience. Vienna, Austria: IAEA, 2006.

[14] J. Brandt, J. H. Christensen, and L. M. Frohn, “Modelling transport and deposition of caesium and iodine from the Chernobyl accident using the DREAM model,” Atmospheric Chemistry and Physics, vol. 2, pp. 397–417, 2002, doi: 10.5194/acp-2-397-2002.

[15] International Atomic Energy Agency (IAEA), Atmospheric Dispersion in Nuclear Power Plant Siting, Safety Series No. 50-SG-S3, Vienna, Austria, 1980; and Dispersion of Radioactive Material in Air and Water and Consideration of Population Distribution in Site Evaluation for Nuclear Power Plants, Safety Standards Series No. NS-G-3.2, Vienna, Austria, 2002.

[16] V. Sinha, M. Atikler, and M. Mileski, “Atmospheric dispersion of radioactive materials for radiological risk assessment in case of a hypothetical sodium-cooled fast reactor accident,” Nuclear Engineering and Design, vol. 422, Art. no. 113124, Jun. 2024.

[17] Z. Ma et al., “Numerical study for atmospheric transport of radioactive materials for a hypothetical severe nuclear accident under different meteorological conditions,” 2024.

[18] M. K. Osman, W. K. Hocking, and D. W. Tarasick, “Parameterization of large-scale turbulent diffusion in the presence of both well-mixed and weakly mixed patchy layers,” Journal of Atmospheric and Solar-Terrestrial Physics, vols. 143–144, pp. 14–36, Jun. 2016.

[19] I. Alrammah, I. M. M. Saeed, M. H. A. Mhareb, and M. Alotiby, “Atmospheric dispersion modeling and radiological environmental impact assessment for normal operation of a proposed pressurized water reactor on the eastern coast of Saudi Arabia,” Progress in Nuclear Energy, vol. 145, Art. no. 104121, Mar. 2022.

[20] International Atomic Energy Agency (IAEA), Meteorological and Hydrological Hazards in Site Evaluation for Nuclear Installations, Safety Standards Series No. SSG-18, Vienna, Austria, 2011.

[21] International Atomic Energy Agency (IAEA), Dispersion of Radioactive Material in Air and Water and Consideration of Population Distribution in Site Evaluation for Nuclear Power Plants, Safety Standards Series No. NS-G-3.2, Vienna, Austria, Mar. 2002.

[22] G. Efthimiou, “An empirical theoretical model for the turbulent diffusion coefficient in urban atmospheric dispersion,” Urban Science, vol. 9, no. 7, Art. no. 281, 2025, doi: 10.3390/urbansci9070281.

[23] NOAA, “READY Gaussian dispersion model,” [Online]. Available: https://www.ready.noaa.gov/READY_gaussian.php